High-pressure geophysical properties of *fcc* phase FeH_X

E. C. Thompson[1,*], A. H. Davis[1], W. Bi[2,3], J. Zhao[3], E. E. Alp[3], D. Zhang[4], E. Greenberg[5], V. B. Prakapenka[5], and A. J. Campbell[1]

[1]University of Chicago, Department of the Geophysical Sciences, Chicago, Illinois, USA.
[2]University of Illinois, Department of Geology, Urbana, Illinois, USA.
[3]Argonne National Lab, Advanced Photon Source, Argonne, Illinois, USA.
[4]University of Hawaii Manoa, Hawaii Institute of Geophysics & Planetology, Honolulu, Hawaii, USA.
[5]Center for Advanced Radiation Sources, University of Chicago, Argonne, IL USA.

*Corresponding author: Elizabeth Thompson (ecthompson@uchicago.edu)

Submitted to *Geochem. Geophys. Geosyst.* August 2, 2017

Accepted by *Geochem. Geophys. Geosyst.* December 26, 2017

Abstract

Face centered cubic (*fcc*) FeH_X was synthesized at pressures of 18 to 68 GPa and temperatures exceeding 1500 K. Thermally quenched samples were evaluated using synchrotron X-ray diffraction (XRD) and nuclear resonant inelastic X-ray scattering (NRIXS) to determine sample composition and sound velocities to 82 GPa. To aid in the interpretation of non-ideal ($X \neq 1$) stoichiometries, two equations of state for *fcc* FeH_X were developed, combining an empirical equation of state for iron with two distinct synthetic compression curves for interstitial hydrogen. Matching the density deficit of the Earth's core using these equations of state requires 0.8-1.1 wt.% hydrogen at the core-mantle boundary and 0.2-0.3 wt.% hydrogen at the interface of the inner and outer cores. Furthermore, a comparison of Preliminary Reference Earth Model (PREM) [Dziewonski and Anderson; 1981] to a Birch's law extrapolation of our experimental results suggests that an iron alloy containing ~0.8 to 1.3 wt.% hydrogen could reproduce both the density and compressional velocity (V_P) of the Earth's outer core.

1 Introduction

Earth's core is composed of an iron-rich alloy with the inclusion of light elements necessary to compensate for the 5-10% difference between seismically determined core densities and the density of pure iron at relevant pressure and temperature (*P-T*) conditions [*Birch*, 1952]. As the most abundant and lightest element in the solar system, hydrogen is a plausible contributor to this core density deficit [e.g., *Williams and Hemley*, 2001]. Iron hydride formation at Earth's surface is unlikely because the equilibrium hydrogen solubility in iron at atmospheric conditions is prohibitively low. However, as hydrogen solubility increases with pressure, so does the likelihood of FeH_X formation within the Earth's interior [*Fukai and Akimoto*, 1983]. Nearly stoichiometric iron hydride (FeH_X, X~1) has been shown to result from either the reaction of Fe and hydrous silicates [*Yagi and Hishinuma*, 1995] or the reaction of Fe and water at lower mantle conditions [*Ohtani et al*., 2005]. Within the known iron hydride phase diagram, the face-centered cubic (*fcc*) structure is considered the most stable structure at high temperatures, rendering it more important for extrapolation to core *P-T* conditions than the *bcc* or *hcp* structures [*Pépin et al*., 2014]. Despite its importance, experimental and *ab initio* efforts have yet to agree on the equation of state parameters needed to describe the compressional behavior of FeH_X [*Fukai et al.,* 2003; *Pépin et al*., 2014; *Hirao*, 2004; *Badding et al.,* 1991]. To constrain the extent to which hydrogen contributes to the density deficit of the Earth's core, it is necessary to establish the compressional wave velocity-density (V_P-ρ) relationship of iron hydrides. New experimentally determined sound velocities of *fcc* FeH_X are reported here. These values are combined with literature values to determine, via Birch's law, the influence of the non-stoichiometric hydrogen on the V_P-ρ relationship of iron.

2 Methods

2.1 Sample synthesis

Two sample geometries were used in this study—one geometry for X-ray diffraction (XRD) experiments only (see Section 2.2), and a second geometry for samples on which both Nuclear resonant inelastic X-ray scattering (NRIXS) and XRD experiments were performed (see Section 2.3). XRD-only samples were composed of a 3-5 μm thick, 30-50 μm diameter natural

iron foil (99.9% purity, Alfa Aesar) pressed between an upper layer of C_nH_{2n+2} paraffin (100% purity, Candlewic), which served as the hydrogen source, and a lower layer of MgO, which served as pressure medium and secondary pressure standard. Paraffin was chosen as a hydrogen source based on the recent successful synthesis of *fcc* FeH demonstrated by *Narygina et al.* [2011]. Additionally, we found no increased occurrence of diamond failure in these samples, presumably indicative of relatively low rates of hydrogen embrittlement. Sample pressures in this geometry were monitored using the Raman shift of the diamond peak [*Akaham and Kawamura*, 2007] and the equation of state for MgO [*Matsui et al.,* 2000]. These XRD-only samples were loaded into Re-gaskets pre-indented to ~27 GPa. In the second geometry, samples were composed of individual 3-5 μm thick, 30-50 μm diameter iron foils of 20-95% ^{57}Fe enrichment (>98% purity, Cambridge Isotope Laboratories) pressed between two layers of C_nH_{2n+2} paraffin (100% purity, Candlewic) that served as both hydrogen source and pressure medium. A small (<10 μm) ruby ball was included in the sample chamber adjacent to the iron foil, to enable pressure determination via the established pressure dependence of the ruby R_1 luminescence line [*Mao et al.* 1986]. These samples, prepared for both XRD and NRIXS experiments, were loaded into pre-indented Be-gaskets with boron-epoxy inserts. Samples of both configurations were loaded into ~70 micron sample chambers in pre-indented gaskets, using panoramic or symmetric diamond anvil cells with 150-300 μm culet anvils.

2.2 Synchrotron X-ray diffraction

Double-sided laser-heating synthesis was performed at beamline 13-ID-D (GSECARS) at the Advanced Photon Source (APS) of Argonne National Laboratory, where the formation of *fcc* FeH_X was monitored using *in situ* angle-dispersive XRD. Samples were simultaneously laser-heated on both sides using a flat-top profile laser, and laser power was adjusted upstream and downstream throughout heating to minimize axial temperature gradients, such that upstream/downstream differences were ~4% of the sample temperature. Temperatures were determined via spectroradiometry using the greybody approximation [*Prakapenka et al.*, 2008]. Diffraction measurements utilized a monochromatic incident X-ray beam (λ = 0.3344 Å or 0.2952 Å) with a 3 μm by 4 μm focus size at full-width at half-maximum. Additional details of sample synthesis including *P–T–V* information can be found in Table S1. Sample-to-detector distances and tilt were calibrated using 1-bar diffraction of LaB_6. DIOPTAS was used to produce 2θ plots [*Prescher and Prakapenka*, 2015], and PeakFit [*Systat Software*] was used to fit individual Gaussian peaks in the resultant integrated patterns to determine lattice parameters as a function of pressure.

Pre-heating XRD confirmed that initial sample foil composition at high pressure was *hcp* iron, and *in situ* high-temperature diffraction established the formation of *fcc* FeH_X at temperatures of, or exceeding, 1500 K (Table S1). Although the peak synthesis temperatures of this study at times exceeded the melting curve reported by *Sakamaki et al.* [2009], this discrepancy may be attributed to the different eutectic melting systems in these studies, which were on opposite sides of the FeH composition. High *P-T* conditions were held until all *hcp* iron peaks diminished, at which point the sample was thermally quenched by shutting off laser power. Post-heating room-temperature patterns were evaluated to confirm quenching of *fcc* FeH_X (Figure 1). Pre- and post-heating sample pressures determined using the Raman shift of the diamond peak revealed a post-heating pressure decrease (~0.5 GPa), consistent with the transition to a higher density phase. The reaction sequence previously described by *Narygina et al.* [2011] (Fe

+ $C_nH_{2n+2} \rightarrow 2Fe_3C + 3H_2 \rightarrow 6FeH + 2C$) was not consistently observed, as no attempt was made to evaluate this transformation with low temperature (<1500 K) diffraction. Additionally, the obtained phase assemblage (Table S1) did not consistently indicate the presence of diamond, likely due to diamond's poor diffraction properties, particularly when synthesized at low temperatures [*Zeng et al*. 2017]. Though the formation of *fcc* FeH_X could be confirmed using at minimum the (111) and (200) peaks, the presence of iron carbide was not detected via XRD.

2.3 Nuclear resonant inelastic X-ray scattering (NRIXS)

Sample synthesis for NRIXS experiments relied on the sample geometry described previously in 2.1 in panoramic-type diamond anvil cells. After starting materials were loaded, FeH_X was synthesized at the University of Chicago via single-sided laser heating with a 1064 nm Yb-doped fiber laser. Temperatures were determined by multispectral imaging radiometry [Campbell 2008] and reported uncertainties reflect the temperature gradient typical of one-sided laser heating of a thin foil sample. To homogenize the synthesized sample the laser, producing a ~15 μm diameter heated spot, was slowly rastered across the sample chamber, avoiding the outermost edges nearest the gasket. Post-synthesis synchrotron XRD to confirm the conversion of iron to *fcc* FeH_X and evaluate sample stoichiometry was performed at 13-ID-D (as previously described) or at 13-BM-C using a monochromatic incident X-ray beam (λ = 0.434 Å). Initially, diffraction patterns were obtained at each post-synthesis pressure step to monitor stoichiometric changes in the quenched sample. In the final sample this was deemed unnecessary as the stoichiometry of each sample was found to depend solely on the *P-T* conditions of formation and not post-quench pressure changes.

Ambient temperature NRIXS experiments on thermally quenched *fcc* FeH_X were performed at Sector 3 of APS, Argonne National Laboratory. NRIXS spectra were obtained using an incident X-ray energy tuned within ±100 meV around the nuclear transition energy of ^{57}Fe (14.4125 keV), an X-ray beam of approximately 15 μm diameter (FWHM) and an energy resolution of 1 meV in the first experimental run and 2 meV in the second run. Three avalanche photodiode detectors, positioned equidistantly around the panoramic DAC, collected time-delayed $K_{\alpha,\beta}$-fluorescence emitted from the excitation of the enriched iron sublattice due to the incident X-ray beam. The storage ring was operated in top-up mode with 24 bunches separated by 153 ns, allowing for the detection of nuclear resonant scattering during the time window following initial excitation. Multiple ~45 minute NRIXS scans were collected at each pressure step and stacked to maximize counts with total per sample accumulation times of 10-21 hours, increasing the signal to noise ratio. The collected *fcc* FeH_X spectral form was found to be distinct from that of pure Fe or *dhcp* FeH_X. Stacked spectra were analyzed using both PHOENIX [*Sturhahn*, 2000] and Sciphon 1.0.3 [*Dauphas et al*., 2014] to extract the partial phonon density of states (pDoS) from the iron sublattice using a quasiharmonic model (Figure 1b).

2.4 Synchrotron Mössbauer spectroscopy (SMS)

Room-temperature forward scattering synchrotron Mössbauer spectra of thermally quenched *fcc* FeH_X samples were collected at beamline 3-ID-B of the Advanced Photon Source, Argonne National Laboratory using a fourth detector in line with the incident X-ray beam path. These experiments were performed contemporaneously to 64 and 82 GPa NRIXS measurements using the same samples. A thin plate of $FeSO_4 \bullet 7H_2O_4$ (IS = 1.34 mm/s, QS = 3.16 mm/s) introduced into the beam path was used as a reference to obtain the isomer (central) shift. Resultant SMS spectra were evaluated using the CONUSS program [*Sturhahn*, 2000] to

determine the magnetic properties, isomer shift, and quadrupole splitting of *fcc* FeH_X as a function of pressure (Figure S2).

3 Results

3.1 Equation of state and sample stoichiometry

Determining the stoichiometry of metal hydrides is difficult owing to the small X-ray cross-section of hydrogen. However, it is possible to make informed estimates of the amount of hydrogen dissolved in the phase based on cell volumes and the well-established behavior of pure *fcc* iron. Hydrogen content of FeH_X can be estimated using the formula:

$$x = \left(V_{FeHx} - V_{Fe}\right) / \triangle V_H \tag{1}$$

in which V_{FeHX} and V_{Fe} are unit cell volumes of iron hydride and pure iron metal, respectively, and ΔV_H is a predetermined volume expansion due to a single formula unit of interstitial hydrogen. The value of ΔV_H is not precisely known for iron hydrides, and previous studies have utilized fixed values ranging from 1.8 to 2.6 Å^3 [*Antonov et al*., 1998; *Badding et al.,* 1991; *Fukai et al*., 2005; *Narygina et al*., 2011]. The basis for these approximations is the interstitial volumes associated with other *3d*-transition metal hydrides or deuterides [e.g., CoH; *Fukai et al.*, 2005]. Variations in ΔV_H can substantially alter the assumed stoichiometry of a sample, and the assumption that this value is fixed across all pressures may result in erroneous equations of state.

This study instead leverages more realistic interstitial hydrogen volumes that vary as a function of pressure. We utilize two different interstitial hydrogen equations of state, one based on *hcp* FeH_X calculations of *Caracas* [2015] and one based on the experimental *dhcp* FeH results of *Pépin et al.* [2014]. No comparable work on the equation of state of *fcc* FeH is available, so we rely on the interstitial H volume in these closely related structures. In both cases, the *V-P* relationship of interstitial hydrogen in FeH_X was determined by evaluating the difference in volume between the volumes of iron hydride and pure *hcp* iron at the same pressure. The reference volume of pure iron used with the Caracas [2015] dataset was the iron curve presented in that same work, while an empirical equation of state by *Dewaele et al.* [2006] was used for the *Pépin et al.* [2014] dataset. This synthetic *V-P* data for hydrogen in FeH_X was fit to a third-order Birch-Murnaghan (BM) equation of state [*Birch*, 1978]:

$$P(V,T) = 3K_0 f_E \left[\left(1+2f_E\right)^{\frac{5}{2}} \left(1 + \frac{3}{2}\left[K_0' - 4\right] f_E\right)\right] \tag{2}$$

which relates pressure (P), volume (V), ambient pressure bulk modulus (K_0), and its pressure derivative (K_0') in terms of finite Eulerian strain (f_E):

$$f_E = \frac{1}{2}\left[\left(\frac{V_0}{V}\right)^{\frac{2}{3}} - 1\right] \tag{3}$$

which is a measure of the volume compression of a solid relative to its initial volume (V_0). The resultant equation of state parameters for interstitial hydrogen in iron hydrides are reported in Table 1. A known trade-off exists between reference volume (V_0) and bulk modulus (K_0), such

that both experimentally and theoretically grounded equations of state provide reasonable, and not dissimilar, estimates of interstitial hydrogen compressibility.

The two interstitial hydrogen equations of state were combined with an experimental equation of state (EoS) for *fcc* iron [*Tsujino et al*., 2013] to enable the determination of sample stoichiometry in our experiments (Figure 2, Table S1), using equation (1) with ΔV_H from the equations of state for interstitial H in FeH_X (Table 1). While the stoichiometries of our samples cluster around X=1, there is scatter, particularly in at low pressures (<35 GPa). No systematic co-variation was observed linking temperature of synthesis, heating duration, or sample geometry to stoichiometry. It is possible that local variation, at the scale of the laser heated spot, in the paraffin:Fe ratio of the sample led to reduced hydrogen enrichment at some *P-V* points. These sample stoichiometries were subsequently used to interpret the resultant phonon density of states and Mössbauer hyperfine field parameters. Here it is assumed that ΔV_H is identical in both *fcc* and *hcp* FeH, because of the similarity of interstitial sites in these structures. Based on the congruence of FeH_X volumes and inferred stoichiometries (and velocities, described below) presented herein and earlier work in carbon-free (with respect to starting materials) Fe-H systems [e.g. *Mao et al*., 2004], we infer that during synthesis only negligible amounts of carbon entered the iron hydride.

In addition to evaluating the stoichiometry of our own samples, our synthetic FeH equations of state based on combining the EoS of pure *fcc* iron [*Tsujino et al*., 2013] with the addition of hydrogen determined both theoretically and experimentally [*Caracas*, 2015; *Pépin et al.,* 2014] were used to reevaluate the previously published EoS of *fcc* FeH_X by *Narygina et al*. [2011] (Figure 2b). This comparison illuminates an important discrepancy as shown in Figure 2a, namely that the *Narygina et al*. [2011] EoS requires the interstitial hydrogen to exhibit a negative bulk modulus, as the volume difference between their FeH isotherm and that of pure *fcc* iron increases with increasing pressure. The results of *Narygina et al.* [2011] might instead be better interpreted as a pressure-dependent evolution of stoichiometry, an interpretation that could also explain the unusually large bulk modulus pressure derivative (K'=11.7) reported in their study.

3.2 Nuclear hyperfine interactions

Synchrotron Mössbauer spectra of *fcc* FeH_X at 64 and 82 GPa consist of a single broad feature (Figure S1). The 64 GPa hyperfine fields were best fit by model with a single iron sublattice site while the 82 GPa hyperfine fields were best fit by a model with a second site, consistent with a slightly distorted cubic system, possibly due to the room-temperature compression of the sample post-synthesis. The quadrupole splitting (QS) of a material using SMS is determined by fitting the experimental spectra to a model, and is indicative of the degree to which an electric field gradient has caused nuclear splitting in the iron sublattice, and to a lesser extent, the coordination of iron. If present, a pressure-induced spin transition (HS → LS) would lead to a dramatic increase in the value of QS [*Li et al.,* 2006; *Bengsten et al., 2009*; *Catalli et al.,* 2011; *Hsu et al.,* 2011], but as no such change in the value of QS between the 64 and 82 GPa spectra from this experiment (Table 1) a spin transition appears unlikely in *fcc* FeH_X in this pressure range. Spectra at both pressures have similar (isomer) central shifts (CS) with respect to α-iron at comparable pressure, are in reasonable agreement with the CS previously reported by *Narygina et al.* [2011] at 47 GPa, and are distinct from the central shift reported for either the *dhcp* or *hcp* phases (Table S2). In agreement with previous studies, the *fcc* phase of

FeH_X is not ferromagnetic, in contrast to that of the *dhcp* and *hcp* phases [*Narygina et al*., 2011; *Tsumuraya et al*., 2012], and as such SMS functions as a secondary confirmation of the structure of our samples, as there is no evidence of magnetic hyperfine field splitting in the measured spectra.

3.3 Sound velocities and geophysical parameters

Coupled with quasi-hydrostatic XRD data and two *fcc* FeH equations of state to provide appropriate parameters, NRIXS provides velocity-density (V_P-ρ) information for comparison against seismic measurements. The Debye velocity (V_D) was determined from the calculated pDoS using both PHOENIX [*Sturhahn*, 2000] and Sciphon [*Dauphas et al*., 2014], assuming Debye-like behavior at low energies and fitting the low energy (~3.8 to 16.2 meV) region to a parabola (Table 2). Once a Debye velocity was obtained by fitting the partial phonon density of state curve, additional equation of state information was incorporated to extract compressional (V_P) and shear velocities (V_S) using the following equation [*Mao et al*., 2001]:

$$\frac{3}{V_D^3} = \frac{1}{V_P^3} + \frac{2}{V_S^3} \tag{4}$$

In this study, the necessary input parameters (K, ρ), as well as stoichiometric information, were obtained from the two previously described FeH_X equations of state. The shear moduli (μ) are fit using the sample density and shear velocity, based on the definition $\mu = \rho V_S^2$. Sound velocities as determined from PHOENIX software are reported in Table 2; comparable values determined using Sciphon, as well as the mean interatomic force constants (Φ) and Lamb-Mössbauer factor (f_{LM}), are included in Table S2. These parameters help to constrain the density, velocities, and moduli of *fcc* FeH_X for comparison to seismic observations of Earth's core.

4 Hydrogen in the core

The Earth's core is known to be lighter than pure iron at the corresponding pressures and temperatures [*Birch*, 1952]. The density deficit has been estimated to be 5–10% for the outer core [*Stevenson*, 1981; *Anderson and Isaak*, 2002] and 1–2% for the inner core [*Jephcoat and Olson*, 1987; *Stixrude et al.,* 1997], attributable to the presence of one or more light element-bearing component(s) in the Earth's core. In addition to other elements (O, S, C, Si, etc.), hydrogen has long been considered a potentially major light component in the core [e.g.; *Stevenson*, 1977]. The amount of hydrogen needed to fulfill the density deficit can be estimated assuming an ideal mixture of pure iron and light element-bearing phases, and extrapolating the corresponding equations of state (EOSs) to core-mantle boundary (CMB) conditions [*Poirier*, 1994].

High-temperature Birch-Murnaghan EoSs for *fcc* iron [*Tsujino et al*., 2013] and *hcp* iron [*Dewaele et al.*, 2006] were combined with our theoretically-based interstitial hydrogen equations of state (Table 1) to determine the necessary hydrogen content required to match the density of PREM at the CMB and at the inner core boundary (ICB) in *fcc* and *hcp* iron hydrides. While these synthetic equations of state reflect the thermal expansion of the iron component, no additional adjustment was made to mimic the potential thermal expansion of the interstitial hydrogen, as this relationship is unconstrained. To our knowledge no experimental measurements

of the density of liquid FeH_X exist, and approximations made on the basis of the known behavior of solids are the best available estimates. All CMB density calculations included a δV of +1.5% due to melting [*Anderson and Isaak*, 2000] and used CMB temperatures of 4000±500 K [*Anderson*, 2003]. Based on these calculations, the density at the CMB can be matched by an *hcp* iron hydride alloy of 1.0–1.3 wt.% hydrogen or an *fcc* alloy containing 0.8-1.1 wt.% hydrogen. A similar density calculation was made to determine the maximum hydrogen content of the Earth's inner core based on matching PREM ICB density, using an ICB temperature of 5500±500 K [*Anderson*, 2003]. This calculation indicated the ICB density can be matched an *hcp* iron hydride alloy of 0.4-0.6 wt.% hydrogen or an *fcc* alloy containing 0.2-0.3 wt.% hydrogen. Although the accuracy of the *fcc* iron equation of state is sufficient to determine the hydrogen contents in our FeH_X samples, which are close in pressure to the stability range of *fcc* iron, the extrapolation of the *fcc* equation of state to Earth core conditions is significant. As such, hydrogen core-content estimates calculated using an *hcp* iron hydride alloy calculation to match PREM densities at the CMB and ICB (1.0–1.3 wt.% and 0.4-0.6 wt.%, respectively) are likely more accurate, as the *hcp* iron *P-V-T* relationship has been assessed up to inner core pressures.

Birch's law, effectively a linear extrapolation of the compressional wave velocity-density (V_P-ρ) relationship, has long been used to assess potential core constituent light elements [e.g., *Badro et al*., 2007]. As hydrogen incorporation into the Earth's inner core is likely below 2 wt.%, our sound velocities of nonstoichiometric *fcc* FeHx, as well as literature data for additional structures of FeHx, were used to extrapolate the effect of hydrogen incorporation of FeH_X, using the relationship:

$$V_P = a + b\rho + cX \tag{5}$$

in which V_P is in units of km · s^{-1}, density (ρ) is in units of kg · m^{-3}, and stoichiometry (X) is in formula units. Two methods were used for this calculation. The first method fit experimental iron hydride data only [*this study*; *Shibazaki et al.* 2012; *Mao et al.* 2004], holding the values of a and b fixed to -4000(11) m · s^{-1} and 1.206(11) m^4 · kg^{-1} · s^{-1} respectively, adopting values reported by *Antonangeli and Ohtani* [2015] to describe the linear V_P-ρ relationship in pure iron which persists up to the pressure of Earth's inner core. In the second method, experimental iron hydride data [*this study*; *Shibazaki et al.* 2012; *Mao et al.* 2004], and *hcp* iron data [*Antonangeli et al.* 2012; *Ohtani et al.* 2013], were fitted together to the above equation, solving for all three parameters (a, b and c). Literature data for FeH_X were reassessed using the equations of state presented herein for self-consistency within these Birch's law parameterizations, including adjustments to stoichiometry, density, V_S and, in the case of NRIXS data, V_P. These two methods were repeated using NRIXS V_P results determined using both interstitial hydrogen equations of states reported in Table 1, and results of these Birch Law calculations are reported in Table 3 and Table S3.

An example of the first method is shown in Figure 3, in which the influence of hydrogen incorporation is added to the previously determined (V_P-ρ) relationship reported by Antonangeli and Ohtani [2015], and only the new variable hydrogen stoichiometry parameter (c) is fit to Eq. 5. The resultant values of c reported herein reflect a significant influence of interstitial hydrogen on the V_P-ρ relationship of iron hydrides. The magnitude of this influence (i.e., values of c) are indistinguishable to those reported by Umemoto and Hirose [2015] based on molecular dynamics calculations. Similarly, the experimentally determined shear wave velocities (V_S) from this study

were combined with literature values [*Shibazaki et al.* 2012; *Mao et al.* 2004; *Mao et al.* 1998; *Lin et al.* 2005] to parameterize the influence of interstitial hydrogen on the shear wave velocity-density (V_s-ρ) relationship in iron hydrides (Equation S1, Table S4, Figure S2). The differences in *Vs* of FeH_X between studies are much higher than for *Vp*, and furthermore the unknown temperature effect on *Vs* is likewise greater than for *Vp*; consequently only the V_P-ρ parameterization is relied upon below to place limits on the inner core's hydrogen content.

Applying our Birch's Law parameterization (line 1 in Table 3) to ICB conditions suggests hydrogen incorporation is irreconcilable with attempts to simultaneously match the density and compressional sound velocity of Earth's inner core, as hydrogen leads to increased values of V_P relative to pure iron at a given density (Figure 3). However, this is an incomplete view, as increased temperature has been shown to have the opposite effect - i.e., pure iron (X=0) at high temperatures has reduced sound velocities relative to 300 K iron at a fixed density [*Decremps et al*., 2014; *Antonangeli et al.*, 2012; *Lin et al*., 2005]. Yet, although the literature reflects consensus on the general effect of temperature on the V_P-ρ relationship of iron, the magnitude and linearity of this effect remains contested [e.g., *Antonangeli et al.* 2012; *Lin et al*., 2005]. Since there is no agreed upon temperature effect, here we evaluate the interplay between dV_P/dT and the amount of hydrogen needed to satisfy PREM. To quantify this, a linear temperature effect (d), was added to the previously defined FeH_X V_P-ρ relationship (Eq. 5):

$$V_P = a + b\rho + cX + d(T\text{-}300) \quad (6)$$

in which temperature (T) is in kelvin. The utility of adding a temperature-dependence term to a 300 K Birch's Law fitting has been previously demonstrated [e.g., *Ohtani et al*., 2013]. Using Eq. 6, we evaluated the amount of hydrogen needed to reproduce PREM ICB density and compressional velocity at an ICB temperature of 5500±500 K (Figure 4). As shown in Figure 4, the greater the V_P reduction caused by high temperatures, the more hydrogen could be incorporated into the Earth's inner core while satisfying the density and velocity of PREM. It is unlikely that hydrogen could be the sole light element in Earth's core, because other candidate components (Si, O, S) are known to dissolve into the metal to varying degrees at high pressures and temperatures (Fischer et al., 2015). However, as shown in Figure 4, a hydrogen content of ~0.8 to 1.3 wt.%, which satisfies the core density deficit as described above, also matches the V_P profile of the inner core if the mean thermal reduction in velocity is -0.22 to -0.31 m s^{-1} · K^{-1} for the Fe-H alloy. This further illustrates that additional high temperature sound velocity measurements of solid iron and iron alloys are greatly needed to more accurately predict the light element content of Earth's core.

Acknowledgments

The authors declare no real or perceived financial conflicts of interest related to this work. Supporting information can be found in the supplemental documents. The authors thank our anonymous reviewers who provided critical feedback that vastly improved the quality of this manuscript. This work was supported by the National Science Foundation under Grants DGE-1144082 and EAR-1427123. This research was completed at Sector 3 and Sector 13 of the Advanced Photon Source. GeoSoilEnviroCARS (Sector 13) is supported by the National Science Foundation (EAR-1128799) and Department of Energy (DE-FG02-94ER14466). Some measurements were performed at the 13-BM-C experimental station of the GSECARS facility at

the APS. 13-BM-C operation is supported by COMPRES through the Partnership for Extreme Crystallography (PX^2) project, under NSF Cooperative Agreement EAR 11-57758. Portions of the synthesis were performed at HPCAT (Sector 16), which are supported by DOE-NNSA under Award No. DE-NA0001974 and DOE-BES under Award No. DE-FG02-99ER45775, with partial instrumentation funding by NSF. This research used resources of the Advanced Photon Source, a U.S. Department of Energy (DOE) Office of Science User Facility operated for the DOE Office of Science by Argonne National Laboratory under Contract No. DE-AC02-06CH11357. W.B. acknowledges partial support from COMPRES, the Consortium for Materials Properties Research in Earth Sciences under NSF Cooperative Agreement No. EAR 1606856.

References

Akahama, Y., and Kawamura, H. (2007) Diamond anvil Raman gauge in multi-megabar pressure range. High Press. Res., 27(4), 473-482. DOI: 10.1080/08957950701659544.

Anderson, O.L., and Isaak, D.G. (2000) Calculated melting curves for phases of iron. Am. Mineral., 85, 376–385. DOI: 10.2138/am-2000-2-317.

Anderson, O.L., and Isaak, D.G. (2002) Another look at the core density deficit of Earth's outer core. Phys. Earth Planet. Inter., 131, 19–27. DOI: 10.1016/S0031-9201(02)00017-1.

Anderson, O.L. (2003) The three-dimensional phase diagram of iron. V. Dehand, K.C., Creager, S.-I. Karato, S. Zatman (Eds.), Earth's Core: Dynamics, Structure, Rotation, American Geophysical Union, Washington, DC.

Antonangeli, D., Komabayashi, T., Occelli, F., Borissenko, E., Walters, A.C., Fiquet, G. and Fei, Y. (2012) Simultaneous sound velocity and density measurements of hcp iron up to 93 GPa and 1100 K: An experimental test of Birch's law at high temperatures. Earth. Planet. Sci. Lett., 331-332, 210-214. DOI: 10.1016/j.epsl.2012.03.024.

Antonangeli, D., Morard, G., Schmerr, N.C., Komayashi, T., Krisch, M., Fiquet, G. and Fei, Y. (2015) Toward a mineral physics reference model for the Moon's core. Proc. Nat. Acad. Sci. 112(13), 3916-3919. DOI: 10.1073/pnas.1417490112.

Antonangeli, D., and Ohtani, E. (2015) Sound velocity of hcp-Fe at high pressure: experimental constraints, extrapolations and comparison with seismic models. Prog. Earth Planet. Sci., 2:3. DOI: 10.1186/s40645-015-0034-9.

Antonov, V., Cornell, K., Fedotov, V., Kolesnikov, A., Ponyatovsky, E., Shiryaev, V., and H. Wipf (1998) Neutron diffraction investigation of the dhcp and hcp iron hydrides and deuterides. J. Alloys Compd., 264, 214–222. DOI: 10.1016/S0925-8388(97)00298-3.

Badding, J.V., Hemley, R.J., and H-.K. Mao (1991) High-pressure chemistry of hydrogen in metals: In situ study of iron hydride, Science, 80(253), 421–424. DOI: 10.1126/science.253.5018.421.

Badro, J., Fiquet, G., Guyot, F., Gregoryanz, E., Occelli, F., Antonangeli, D., and M. d'Astuto (2007) Effect of light elements on the sound velocities in solid iron: Implications for the

composition of Earth's core, Earth Planet. Sci. Lett., 254, 233–238. DOI: 10.1016/j.epsl.2006.11.025.

Bengstson, A., Li, J., and D. Morgan (2009) Mössbauer modeling to interpret the spin state of iron in (Mg,Fe)SiO_3 perovskite. Geophys. Res. Lett. 36, L15301. DOI: 10.1029/2009GL038340.

Birch, F. (1952) Elasticity and constitution of the Earth's interior. J. Geophys. Res., 57, 227–286. DOI: 10.1029/JZ057i002p00227.

Birch, F. (1978) Finite strain isotherm and velocities for single crystal and polycrystalline NaCl at high-pressures and 300 K. J. Geophys. Res., 83, 1257–1268. DOI: 10.1029/JB083iB03p01257.

Campbell, A.J. (2008) Measurement of temperature distributions across laser-heated samples by multispectral imaging rediometry. Rev. Sci. Instrum., 79. DOI: 10.1063/1.2827513.

Caracas, R. (2015) The influence of hydrogen on the seismic properties of solid iron. Geophys. Res. Lett., 42. DOI: 10.1002/2015GL063478.

Catalli, K., Shim, S.-H., Dera, P., Prakapenka, V.B., Zhao, J., Sturhahn, W., Chow, P., Xiao, Y., Cynn, H., and W.J. Evans (2011) Effects of the Fe^{3+} spin transition on the properties of aluminous perovskite – New insights for lower-mantle seismic heterogeneities. Earth Planet. Sci. Lett., 310, 293-302. DOI: 10.1016/j.epsl.2011.08.018.

Dauphas, N., Roskosz, M., Alp, E.E., Neuville, D.R., Hu, M.Y., Sio, C.K., Tissot, F.L.H., Zhao, J., Tissandier, L., Médard, E. and C. Cordier (2014) Magma redox and structural controls on iron isotope variations in Earth's mantle and crust. Earth Planet. Sci. Lett., 398, 127–140. DOI: 10.1016/j.epsl.2014.04.033.

Dewaele, A., Loubeyre, P., Occelli, F., Mezouar, M., Dorogokupets, P.I., and M. Torrent (2006) Quasihydrostatic equation of state of Iron above 2 Mbar. Phys. Rev. Lett., 97, 29–32. DOI: 10.1103/PhysRevLett.97.215504.

Decremps, F., Antonangeli, D., Gauthier, M., Ayrinhac, S., Morard, M., le Marchand, G., Bergame, F. and Philippe, J. (2014) Sound velocity of iron up to 152 GPa by picosecond acoustics in diamond anvil cell. Phys. Earth Planet. Inter., 41. DOI: 10.1002/2013GL058859.

Dziewonski, A.M., and Anderson, D.L. (1981) Preliminary reference Earth model. Phys. Earth Planet. Inter., 25, 297–356. DOI: 10.17611/DP/9991844.

Fukai, Y. and S. Akimoto (1983) Hydrogen in the Earth's Core. Proc. Jpn. Acad., 59, 158–162. DOI: 10.2183/pjab.59.158.

Fischer, R.A., Nakajima, Y., Campbell, A.J., Frost, D.J., Harries, D., Langenhorst, F., Miyajima, N., Pollok, K., and Rubie, D.C. (2015) High pressure metal–silicate partitioning of Ni,

Co, V, Cr, Si, and O. Geochim. Cosmochim. Acta (167), 177–194. DOI: 10.1016/j.gca.2015.06.026.

Fukai, Y., Mori, K., and Shinomiya, H. (2003) The phase diagram and superabundant vacancy formation in Fe-H allows under high hydrogen pressures. J. Alloys Comp., 348, 105-109. DOI: 10.1016/S0925-8388(02)00806-X.

Fukai, Y. (2005), The Metal–Hydrogen System: Basic Bulk Properties, Second ed. Springer, Berlin. (Chapter 4).

Hirao, N. (2004) Compression of iron hydride to 80 GPa and hydrogen in the Earth's inner core. Geophys. Res. Lett., 31, L06616. DOI: 10.1029/2003GL019380.

Hsu, H., Umemoto, K., Blaha, P., and R.M. Wentzcovich. (2010) Spin states and hyperfine interactions of iron in (Mg,Fe)SiO_3 perovskite under pressure. Phys. Rev. Lett., 106, 118501. DOI: 10.1016/j.epsl.2010.02.031.

Jephcoat, A., and P. Olson (1987) Is the inner Core of the Earth pure iron? Nature, 325, 332–335. DOI: 10.1038/325332a0.

Li, J., Sturhahn, W., Jackson, J.M, Struzhkin, V.V., Lin, J.F., Zhao, J., Mao, H.K., and G. Shen. (2006). Pressure effect on the electronic structure of iron in (Mg,Fe)(Si,Al)O_3 perovskite: a combined synchrotron Mössbauer and X-ray emission spectroscopy study up to 100 GPa, Phys. Chem. Miner. 33, 575-585. DOI: 10.1007/s00269-006-0105-y.

Lin, J-.F., Sturhahn, W., Zhao, J., Shen, G., Mao, H-.K. and R.J. Hemley (2005) Sound velocities of hot dense iron: Birch's Law revisited, Science., 308, 1892–1894. DOI: 10.1126/science.1111724.

Mao, H-.K., Xu, J., and P.M. Bell (1986) Calibration of the ruby pressure gauge to 800-Kbar under quasi-hydrostatic conditions, J. Geophys. Res., B91(B5), 4673–4676. DOI: 10.1029/JB091iB05p04673.

Mao, H-.K., Shu, J., Shen, G., Hemley, R.J., Li, B. and A.K. Singh (1998) Elasticity and rheology of iron above 220 GPa and the nature of the Earth's iron core, Nature 396, 741-743.

Mao, H-.K., Xu, J., Stuzhkin, V.V., Shu, J., Hemley, R.J., Sturhahn, W., Hu, M.Y., Alp, E.E., Vocadlo, L., Alfe, D., Price, G.D., Gillian, M.J., Schwoerer-Böhning, Hausermann, D., Eng, P., Shen, G., Giefers, H., Lubbers, R., and G. Wortmann (2001) Phonon density of states of iron up to 153 gigapascals, Science 292, 914-916. DOI: 10.1126/science.1057670

Mao, W.L., Sturhahn, W., Heinz, D.L., Mao, H.-K., Shu, J. and R.J. Hemley (2004) Nuclear resonant x-ray scattering of iron hydride at high pressure, Geophys. Res. Lett., 31, L15618. DOI: 10.1029/2004GL020541.

Matsui, M., Parker, S.C., and M. Leslie (2000) The MD simulation of the equation of state of MgO: Application as pressure calibration standard at high temperature and high pressure, Am. Min., 85, 312-316. DOI: 10.2138/am-2000-2-308.

Narygina, O., Dubrovinsky, L.S., McCammon, C. A., Kurnosov, A., Kantor, I.Y., Prakapenka, V.B., and N.A. Dubrovinskaia (2011) X-ray diffraction and Mössbauer spectroscopy study of *fcc* iron hydride FeH at high pressures and implications for the composition of the Earth's core, Earth Planet. Sci. Lett., 307, 409–414. DOI: 10.1016/j.epsl.2011.05.015.

Ohtani, E., Hirao, N., Kondo, T., Ito, M., and T. Kikegawa (2005) Iron-water reaction at high pressure and temperature, and hydrogen transport into the core, Phys. Chem. Minerals, 32, 77-82. DOI: 10.1007/s00269-004-0443-6.

Ohtani, E., Shibazaki, Y., Sakai, T., Mibe, K., Fukui, H., Kamada, S., Sakamaki, T., Seto, Y., Tsutsui, S., and A.Q.R. Baron. (2013) Sound velocity of hexagonal close-packed iron up to core pressures, Geophys. Res. Lett, 40, 5089-5094. DOI: 10.1002/grl.50992.

Pépin, C., Dewaele, A., and G. Geneste (2014) New iron hydrides under high pressure. Phys. Rev. Lett., 265504, 1–5. DOI: 10.1103/PhysRevLett.113.265504.

Poirier, J.-P. (1994) Light elements in the Earth's outer core: A critical review. Phys. Earth. Planet. Inter., 85, 319-337. DOI: 10.1016/0031-9201(94)90120-1.

Prakapenka, V.B., Kuba, A., Kuznetsov, A., Laskin, A., Shkurikhin, O., Dera, P., Rivers, M.L., and S.R. Sutton (2008) Advanced flat top laser heating system for high pressure research at GSECARS: application to the melting behavior of germanium, High Press. Res., 28, 225–235. DOI: 10.1080/08957950802050718.

Prescher C. and V.B. Prakapenka (2015) DIOPTAS: a program for reduction of two-dimensional X-ray diffraction data and data exploration, High Press. Res., 35, 223–230. DOI: 10.1080/08957959.2015.1059835.

Sakamaki, K., Takahashi, E., Nakajima, Y., Nishihara Y., Funakoshi, K., Suzuki, T., and Fukai, Y. (2009) Melting phase relation of FeHX up to 20 GPa: Implications for the temperature of the Earth's core, Phys. Earth Planet. Inter., 174, 192-201. DOI: 10.1016/j.pepi.2008.05.017.

Shibazaki, Y., Ohtani, E., Fukui, H., Sakai T., Kamasa, S., Ishikaa, D., Tsutsui, S., Baron, A.Q.R., Nishitani, N., Hirao, N. and Takemura, K. (2012) Sound velocity measurements in dhcp-FeH up to 70 GPa with inelastic X-raw scattering: Implications for the composition of the Earth's core, Earth Planet. Sci. Lett., 313-314, 79-85. DOI: 10.1016/j.epsl.2011.11.002.

Stevenson, D.J. (1977) Hydrogen in the Earth's core, Nature, 268, 130-131. DOI: 10.1038/268130a0.

Stevenson, D.J. (1981) Models of the Earth's core, Science, 214, 611–619. DOI: 10.1126/science.214.4521.611.

Stixrude, L., Wasserman, E., and R.E. Cohen (1997) Composition and temperature of Earth's inner core, J. Geophys. Res., 102, 24729–24739. DOI: 10.1029/97JB02125.

Sturhahn, W. (2000) CONUSS and PHOENIX: Evaluation of nuclear resonant scattering data, J. Phys.: Condens. Matter, 16, 149–172. DOI: 10.1023/A:1012681503686.

Tsujino, N., Nishihara, Y., Nakajima, Y., Takahashi, E., Funakoshi, K., and Higo, Y. (2013) Equation of state of γ-Fe: Reference density for planetary cores. Earth Planet. Sci. Lett. 375, 244-253. DOI: 10.1016/j.epsl.2013.05.040.

Tsumuraya, T., Matsuura, Y., Shishidou, T., and T. Oguchi. (2012) First-principles study on the structural and magnetic properties of iron hydride. J. Phys. Soc. Japan. 81, 064707. DOI: 10.1143/JPSJ.81.064707.

Umemoto, K., and K. Hirose (2015) Liquid iron-hydrogen alloys at outer core conditions by first-principles calculations. Geophys. Res. Lett., 325, 332–335. DOI: 110.1002/2015GL065899.

Williams, Q. and R.J. Hemley. (2001) Hydrogen in the deep Earth, Annu. Rev. Earth Planet. Sci., 29, 365-418. DOI: 10.1146/annurev.earth.29.1.365.

Yagi, T., and T. Hishinuma. (1995) Iron hydride formed by the reaction of iron, silicate, and water: Implications for the light element of the Earth's core, Geophys. Res. Lett., 22(14), 1933-1936. DOI: 10.1029/95GL01792.

Zeng, Z., Yang, L., Zeng, Q., Lou, H., Sheng, H., Wen, J., Miller, D.J., Meng, Y., Yang, W., Mao, W.L. and H-.K. Mao. (2017) Synthesis of quenchable amorphous diamond, Nat. Commun., 8, 322. DOI: 10.1038/s41467-017-00395-w.

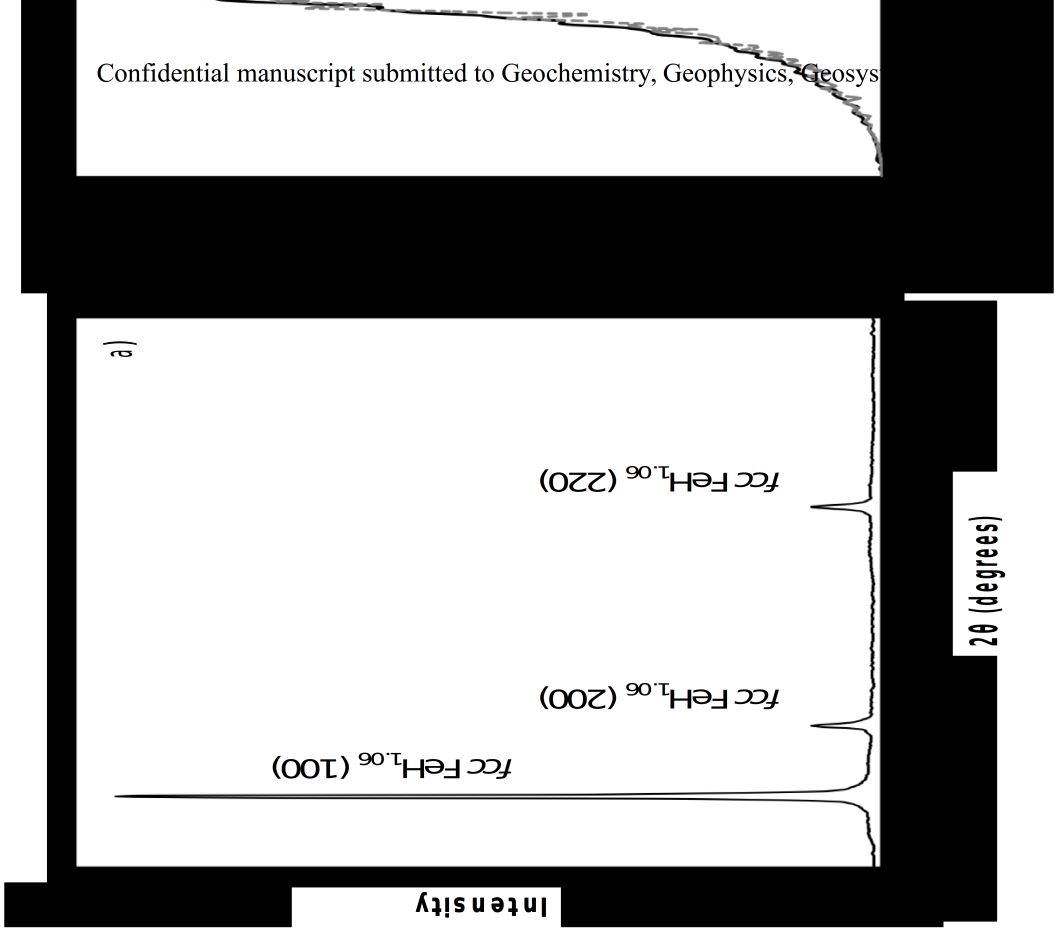

Figure 1. (a) Measurements of quenched non-stoichiometric (X~1.06) *fcc* FeH_X at 64 GPa, including (a) Integrated X-ray diffraction with FeH_X peaks are labeled with their respective Miller indices, and (b) Fe partial phonon density of states (DOS). The DOS indicated by the solid black line was obtained using the PHOENIX program [Sturhahn, 2000], and dotted grey line is the DOS obtained from Sciphon 1.0.3 [Dauphas et al., 2014].

Figure 2. (a) Experimental *P-V* data from this study (black circles) compared to an fcc iron equation of state (blue), a previously reported *fcc* FeH equation of state (grey), and the two new synthetic *fcc* FeH_X equations of state reported in this study, based on Pépin et al., [2014] (red) and Caracas [2015] (orange). Error bars show uncertainty of experimental data points, and when not evident reflect errors not exceeding the size of the symbol itself. (b) Calculated sample stoichiometries of FeH_X as a function of pressure calculated using the hydrogen equation of state based on Pépin et al. [2014] (red solid circles) and Caracas [2015] (open orange triangles). The equation of state for stoichiometric (X=1) *fcc* FeH reported by Narygina et al. [2011] has been re-evaluated using the both synthetic equations of state reported here. Both experimental data and equations of state are plotted at room temperature (300 K).

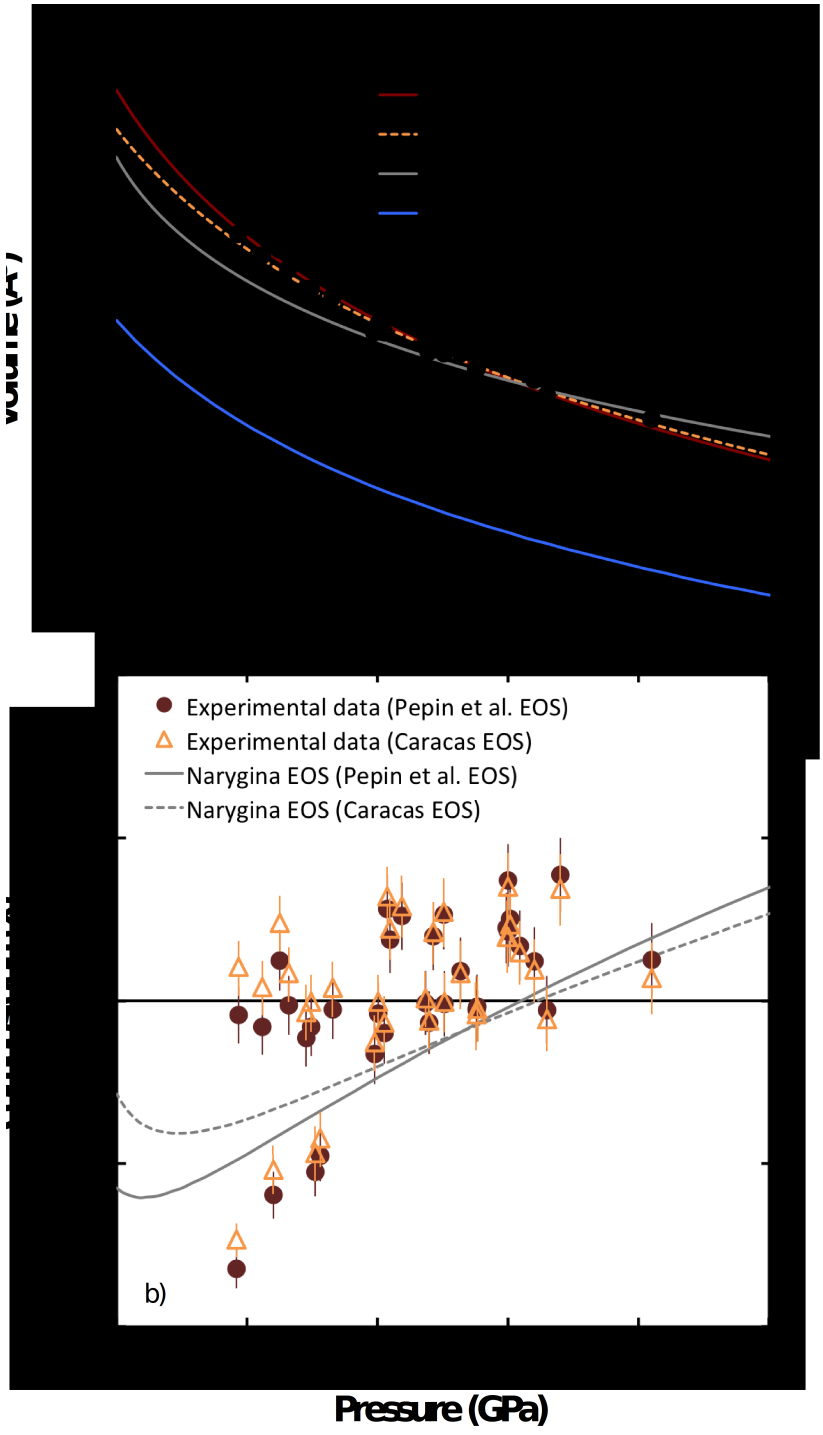

Figure 3. Birch's Law extrapolation of the influence of hydrogen stoichiometry on the velocity-density (V_P-ρ) relationship in iron hydrides. Dotted lines indicate Birch's law parameterization for varying FeH_X stoichiometries, including X=0 (blue), X=0.25 (green), X=0.5 (orange), X=0.75 (red), and X=1 (maroon). Experimental data includes *fcc* FeH_X (triangles), *dhcp* FeH_X (squares), and *hcp* iron (circles) and individual data points have been color coded to reflect the approximate sample stoichiometry. Error bars do not exceed the size of the symbol itself. This fit uses the hydrogen EoS based on Caracas [2015], sound velocities calculated using PHOENIX [Sturhahn, 2000], and Eq. 5. The PREM model for the inner core is represented by crosses and all non-PREM data reflects ambient temperatures. Sample densities as plotted reflect some degree of isotopic variation (i.e., Fe^{57} enrichment) owing to different sample preparation methods.

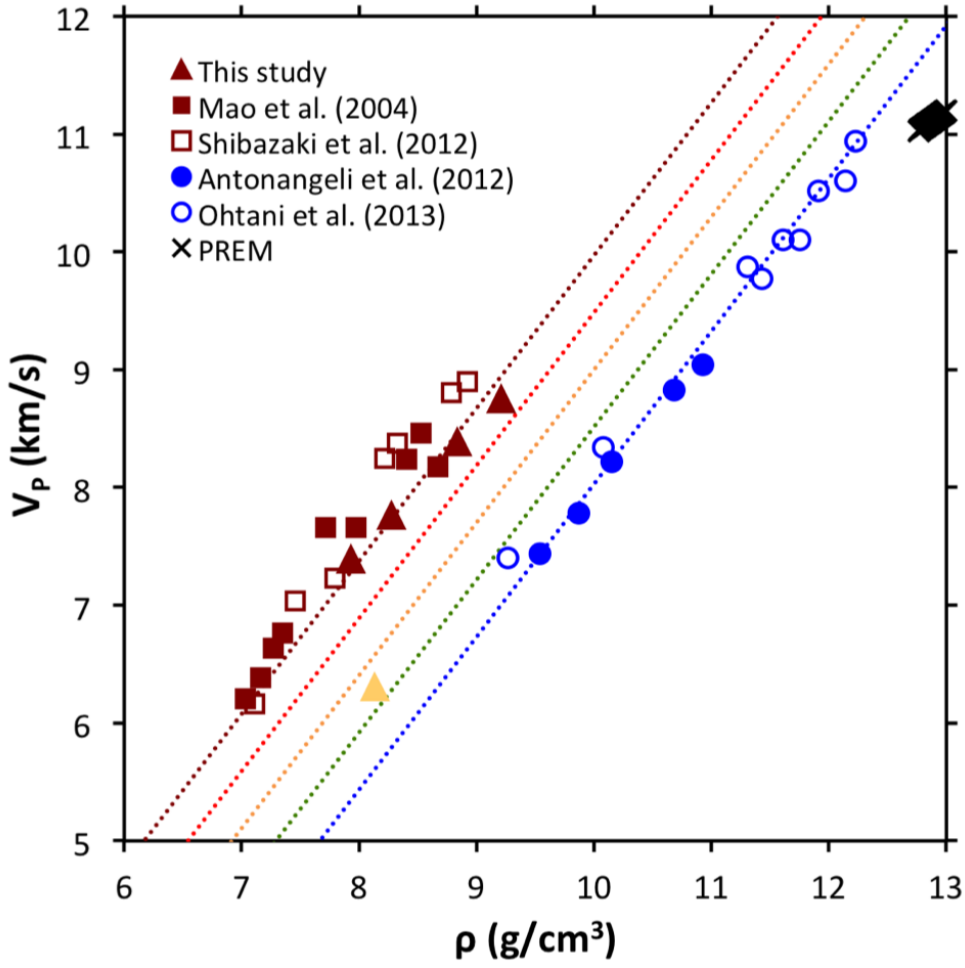

Figure 4. Trade-off between the influence of increased temperature on the compression wave velocity (V_P) of iron and the hydrogen content needed to match the V_P of the inner core boundary (ICB) based on Eq. 6. Modeled hydrogen contents are based on an ICB temperature of 5500 K with error bars reflecting +/- 500K.

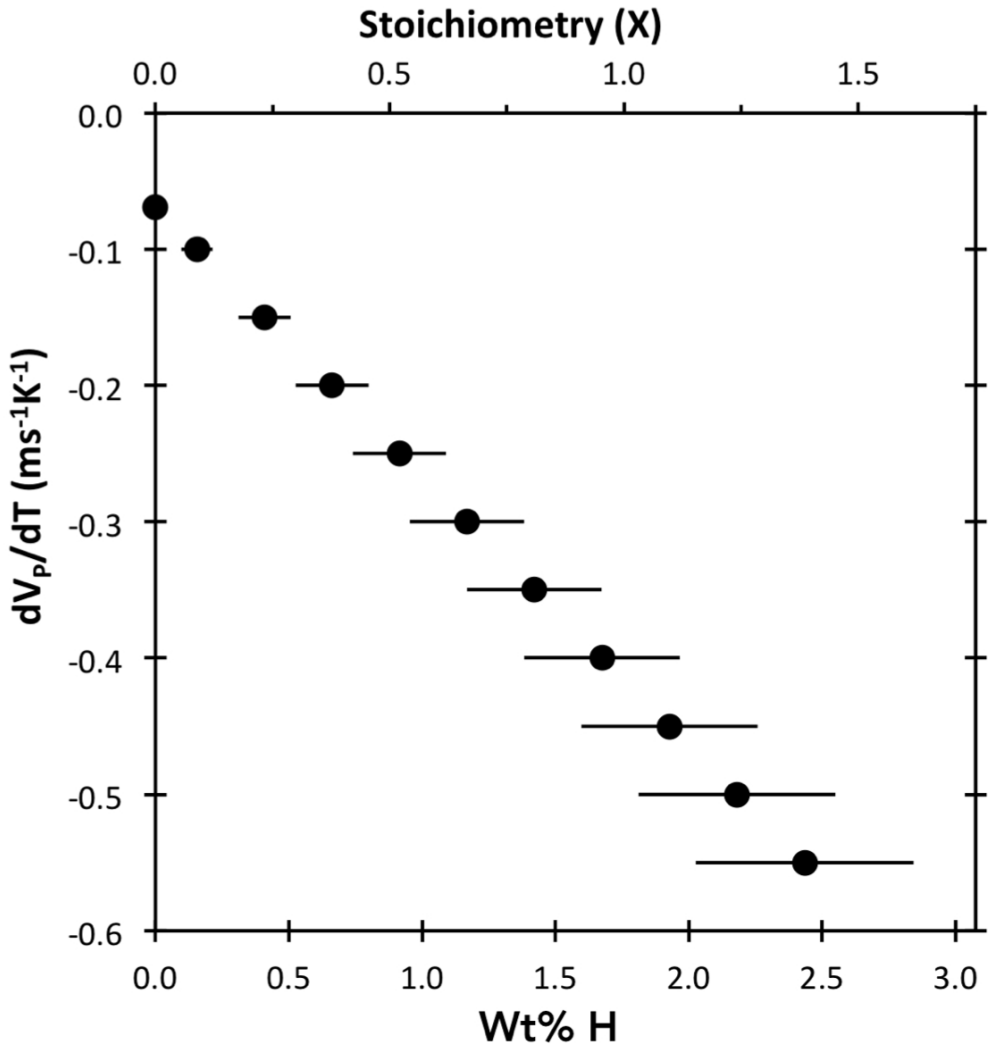

Table 1. Third-order Birch-Murnaghan equation of state parameters for interstitial hydrogen in iron hydride, including ambient-pressure volume (V_0), ambient-pressure bulk modulus ($\boldsymbol{K_0}$) and its pressure derivative ($\boldsymbol{K_0'}$). Values in parentheses are uncertainties in the last digit.

EoS	$\boldsymbol{V_0}$ **(Å^3)**	$\boldsymbol{K_0}$ **(GPa)**	$\boldsymbol{K_0'}$
Based on *Caracas* [2015]	2.232(0)	181.3(1)	3.18(1)
Based on *Pépin et al.* [2014]	2.684(3)	63.14(5)	3.82(1)

Table 2. Geophysically relevant parameters of including sample pressure at time of NRIXS measurement (P), composition in terms of FeH_X (X), density (ρ), bulk modulus (K), shear modulus (μ), compressional wave velocity (V_P), Debye velocity (V_D), and shear wave velocity (V_S) as determined using PHOENIX software. Parameters are shown as calculated using both *fcc* FeH_X equations of state rooted in the Caracas (2015) hydrogen values (denoted as 'C' below) and the Pépin et al. (2014) hydrogen volumes (denoted 'P'). Values in parentheses reflect uncertainties.

P (GPa)	EoS	X	ρ (kg · m^{-3})	K (GPa)	μ (GPa)	V_P (km · s^{-1})	V_D (km · s^{-1})	V_S (km · s^{-1})
18.4(2)	C	0.63(4)	8.14(1)	232(1)	83(1)	6.49(5)	3.59(7)	3.20(7)
18.4(2)	P	0.59(3)	8.14(1)	212(1)	84(1)	6.30(5)	3.59(7)	3.20(7)
29.0(3)	C	0.98(4)	7.94(1)	277(1)	136.5(8)	7.61(2)	4.63(3)	4.15(3)
29.0(3)	P	0.94(4)	7.93(1)	250(1)	137.1(9)	7.39(2)	4.63(3)	4.16(3)
41.0(4)	C	0.97(5)	8.28(1)	326(1)	148.2(9)	7.96(3)	4.73(4)	4.23(4)
41.0(4)	P	0.95(5)	8.28(1)	300(1)	149(1)	7.76(3)	4.73(4)	4.24(4)
64.0(6)	C	1.05(5)	8.83(1)	416(1)	172(1)	8.55(3)	4.94(5)	4.42(5)
64.0(6)	P	1.06(5)	8.83(1)	390(1)	173(1)	8.38(3)	4.94(5)	4.42(5)
82.0(8)	C	1.04(6)	9.21(1)	484(1)	183(1)	8.90(3)	5.01(6)	4.46(5)
82.0(8)	P	1.06(6)	9.21(1)	460(1)	184(2)	8.75(4)	5.00(5)	4.47(5)

Table 3. Birch's law parameters calculated using both *fcc* FeH_X equations of state rooted in the Caracas (2015) (denoted as 'C' below) and the Pépin et al. (2014) (denoted 'P') hydrogen volumes. Input sound velocities (V_P) have been calculated from NRIXS data using PHOENIX [*Sturhahn*, 2000] software, while parameters determined using V_P determined using Sciphon are in Table S2. Values in parentheses are uncertainties in last digit.

EoS	***a* (k · m · s^{-1})**	***b* (m^4 · kg^{-1} · s^{-1})**	***c (dimensionless)***	**Data included in fit**
C	-4 (fixed)	1.206 (fixed)	1.72(8)	This study; Shibazaki et al. 2012; Mao et al. 2004
C	-4 (fixed)	1.206 (fixed)	1.80(7)	This study
C	-5.1(7)	1.31(7)	2.0(2)	This study; Shibazaki et al. 2012; Mao et al. 2004; Antonangeli et al. 2012; Ohtani et al. 2013
P	-4 (fixed)	1.206 (fixed)	1.73(9)	This study; Shibazaki et al. 2012; Mao et al. 2004
P	-4 (fixed)	1.206 (fixed)	1.7(1)	This study
P	-4.9(8)	1.30(7)	1.9(2)	This study; Shibazaki et al. 2012; Mao et al. 2004; Antonangeli et al. 2012; Ohtani et al. 2013